University of Sistan and Baluchestan

Challenges in Nano and Micro Scale Science and Technology

Online ISSN: 2821 - 000X

Catalytic Degradation of Tetracycline in Aqueous Solution Using Cu-Modified γ-MnO_2 Nanostructures

Masoumeh Keramati[1] | Alireza Khorshidi[1]✉

1. Faculty of chemistry, University of Guilan, 41335-1914, Rasht, Iran
Corresponding Author's Email: khorshidi@guilan.ac.ir

Article Info

Article type:
Research Article

Article history:
Received: 2026-06-10
Received in revised form: 2026-06-19
Accepted: 2026-07-01
Published online:

Keywords:
Manganese dioxide,
Tetracycline,
Copper modification,
Heterogeneous catalysis,
Wastewater treatment,

ABSTRACT

Tetracycline antibiotics are among the most recalcitrant micropollutants detected in aquatic environments, posing significant threats to public health due to their low biodegradability, promotion of antibiotic resistance, and endocrine-disrupting potential. In this study, γ-MnO2 and Cu-modified γ-MnO2 (Cu-γ-MnO2) nanostructures were successfully synthesized and evaluated as heterogeneous catalysts for the oxidative degradation of tetracycline in aqueous solution in the presence of H2O2. The synthesized materials were thoroughly characterized by X-ray diffraction (XRD), field-emission scanning electron microscopy (FE-SEM), energy-dispersive X-ray spectroscopy (EDX), and Fourier-transform infrared spectroscopy (FTIR). XRD confirmed the pure γ-MnO2 phase for both materials, with Cu incorporation causing no new crystalline phases but inducing a slight reduction in crystallite size. FE-SEM revealed a unique hedgehog-like morphology with needle-shaped nanocrystals assembled into spherical superstructures (17–36 nm), which was preserved upon Cu modification. Under optimized conditions (pH 4, 55°C, 20 mg catalyst, 1 mL of 30% H2O2, 20 min), Cu-γ-MnO2 achieved 98% tetracycline degradation, significantly outperforming unmodified γ-MnO2 (70%). The reaction followed NLLS biphasic kinetics (k_1 = 1.343 min−1 (R2 = 0.979). The Cu-γ-MnO2 catalyst demonstrated exceptional recyclability, retaining >80% activity after seven consecutive cycles, underscoring its practical feasibility for wastewater remediation applications.

1. INTRODUCTION

The contamination of water resources by emerging organic micropollutants has become one of the most pressing environmental challenges of the twenty-first century. Antibiotics, in particular, have garnered increasing scientific and regulatory attention due to their ubiquitous presence in surface waters, groundwater, and even drinking water supplies [1,2]. Among these, tetracycline antibiotics — including tetracycline (TC), chlortetracycline, oxytetracycline, and doxycycline — are among the most widely used broad-spectrum antibiotics in human medicine, veterinary practice, and aquaculture worldwide [3]. Their extensive use, combined with incomplete metabolic absorption (only 10–50% is metabolized), results in the excretion of 50–90% of administered doses as biologically active compounds into the environment via urine and feces [4].

The persistence of tetracyclines in the environment is a consequence of their highly hydrophilic nature, low volatility, and resistance to conventional biological treatment. Most municipal wastewater treatment plants are poorly equipped to eliminate these contaminants, allowing them to enter receiving water bodies and exert adverse ecological effects. These include the promotion of antibiotic-resistant bacteria and resistance genes — widely recognized as a global public health threat — endocrine disruption in aquatic organisms, and inhibition of microbial communities essential for ecosystem functioning [3,4]. The World Health Organization has classified antibiotic resistance as one of the greatest threats to global health, food security, and development, making the development of effective tetracycline removal technologies an urgent research priority.

Among the various remediation strategies investigated for antibiotic removal from water, advanced oxidation processes (AOPs) have emerged as particularly promising approaches [4]. AOPs are characterized by the *in situ* generation of highly reactive species — principally hydroxyl radicals (•OH) — capable of non-selectively mineralizing recalcitrant organic pollutants. Heterogeneous catalytic oxidation, in which a solid catalyst activates an oxidant such as hydrogen peroxide

How to Cite this paper: Keramati M. Khorshidi A. Catalytic Degradation of Tetracycline in Aqueous Solution Using Cu-Modified γ-MnO_2 Nanostructures. *Challenges in Nano and Micro Scale Science and Technology*. 2026; 14(2): 45-56. DOI: 10.22111/cnmst.2026.55742.1308

 Publisher: University of Sistan and Baluchestan.
DOI: 10.22111/cnmst.2026.55742.1308

(H_2O_2) to generate reactive radicals, is particularly attractive for practical applications due to the ease of catalyst recovery and reuse [5–7].

Manganese dioxide (MnO_2) has attracted considerable interest as a heterogeneous catalyst for AOPs owing to its natural abundance, low cost, environmental benignity, and tunable crystal structure. MnO_2 exists in multiple polymorphic forms (α-, β-, γ-, δ-MnO_2, etc.) distinguished by their tunnel and layer structures, which profoundly influence catalytic performance [14]. Among these, γ-MnO_2 possesses a unique intergrowth structure comprising both (1×1) and (1×2) tunnels, conferring high surface area, structural defects, and superior electrochemical activity [22,25]. The high lattice oxygen mobility and mixed Mn^{3+}/Mn^{4+} valence of γ-MnO_2 facilitate the activation of H_2O_2 through a Fenton-like mechanism, generating •OH radicals responsible for pollutant degradation.

The catalytic activity of MnO_2 can be further enhanced by transition metal doping. Copper (Cu) is particularly well-suited for this purpose due to its multiple oxidation states (Cu^+/Cu^{2+}), which participate synergistically in redox cycles with Mn^{3+}/Mn^{4+}, enhancing H_2O_2 activation and •OH generation [17,26]. The Cu^+/Cu^{2+} cycle acts analogously to the Fe^{2+}/Fe^{3+} cycle in classical Fenton chemistry, decomposing H_2O_2 at significantly broader pH ranges and lower temperatures than traditional Fenton systems.

Despite recent advances, to the best of our knowledge, no prior study has systematically investigated the catalytic performance of Cu-modified γ-MnO_2 with a uniquely hierarchical needle-assembled spherical morphology for tetracycline degradation. The present work offers several key innovations: (i) a facile, scalable synthesis protocol yielding a highly active Cu-γ-MnO_2 catalyst; (ii) an exceptionally low catalyst loading (0.02 g/L), far below most reported systems; (iii) near-complete TC degradation (98%) within only 20 minutes; (iv) pseudo-first-order kinetics with a high rate constant of 0.267 min^{-1}; and (v) demonstrated recyclability for seven cycles. These attributes collectively position Cu-γ-MnO_2 as a highly competitive, cost-effective, and sustainable catalyst for pharmaceutical pollutant remediation. Manganese dioxide-based catalytic systems have been extensively investigated for environmental remediation over the last two decades. Early studies focused on the intrinsic oxidation capability of MnO_2 polymorphs, whereas more recent investigations have emphasized the enhancement of catalytic activity through transition-metal modification and defect engineering. Among the various MnO_2 polymorphs, γ-MnO_2 has attracted considerable attention owing to its mixed tunnel structure, high density of surface defects, and favorable redox properties. Copper modification represents a particularly attractive strategy because Cu species can introduce additional redox-active centers and facilitate electron-transfer processes during oxidant activation. Despite these advances, studies specifically addressing Cu-modified γ-MnO_2 for rapid tetracycline degradation in H_2O_2-based systems remain limited. Therefore, further investigation of the structure–activity relationship and catalytic behavior of Cu-modified γ-MnO_2 nanostructures is warranted.

2. EXPERIMENTAL

2.1. Materials and Instruments

All reagents were purchased from Merck (Darmstadt, Germany) and Sigma-Aldrich (St. Louis, MO, USA) and used without further purification. Deionized water was used throughout all experiments. Infrared spectra were recorded on a Bruker ALPHA FT-IR spectrometer. Morphological characterization was performed using a MIRA II field-emission scanning electron microscope (FE-SEM) equipped with an energy-dispersive X-ray (EDX) detector. UV-Vis absorption spectra were collected on a Biomate 5 dual-beam UV-Vis spectrophotometer. X-ray diffraction (XRD) patterns were acquired on a Philips PW1730 diffractometer using Cu Kα radiation (λ = 1.5406 Å) over a 2θ range of 10–80°. Centrifugation was carried out using a Centrifuge T16 instrument.

2.2. Synthesis of γ-MnO_2 Nanostructures

γ-MnO_2 nanostructures were synthesized by a hydrothermal co-precipitation method. Two solutions were prepared separately: Solution 1 contained 1.3 g of potassium bromate ($KBrO_3$) dissolved in 17.5 mL of deionized water. Solution 2 was prepared by dissolving 1.2 g of manganese(II) sulfate monohydrate ($MnSO_4 \cdot H_2O$) and 1.7 mL of 0.1 M nitric acid in 16 mL of deionized water. Solution 1 was added dropwise to Solution 2 under continuous magnetic stirring. The resulting mixture was transferred to a reflux condenser and heated in an oil bath at 120°C for 24 hours until a black precipitate formed. The precipitate was collected by filtration, washed repeatedly with deionized water until the filtrate reached neutral pH, and dried at 110°C for 12 hours.

2.3. Synthesis of Cu-γ-MnO_2 Nanostructures

Cu-modified γ-MnO_2 (Cu-γ-MnO_2) was prepared by a wet impregnation method. One gram of the as-synthesized γ-MnO_2 was dispersed in 50 mL of 5.7×10^{-3} M copper(II) acetate [$Cu(CH_3COO)_2$] aqueous solution. The suspension was refluxed at 80°C for 24 hours under constant stirring to ensure uniform Cu^{2+} impregnation onto the γ-MnO_2 surface. The resulting solid was collected by centrifugation, washed several times with deionized water, dried at 70°C for 12 hours, and finally calcined at 300°C for 3 hours in air to obtain the final Cu-γ-MnO_2 catalyst.

2.4. Catalytic Degradation Experiments

Catalytic degradation experiments were performed in a 50 mL glass reactor at atmospheric pressure. In a typical experiment, 20 mg of catalyst was dispersed in 20 mL of tetracycline aqueous solution (40 mg/L) at the desired pH. The reaction was initiated by adding 1 mL of 30% H_2O_2 (42.62 mM). The mixture was maintained at the target temperature under magnetic stirring. At predetermined time intervals, aliquots (1 mL) were withdrawn, centrifuged to remove catalyst particles, and the residual tetracycline concentration was determined by UV-Vis spectrophotometry at λ_{max} = 358 nm. Degradation efficiency was calculated as: Yield (%) = $(1 - C_t/C_0) \times 100$,

where C_0 and C_t are the tetracycline concentrations at time 0 and t, respectively. The pH was adjusted using 1 M HCl or ammonia solution prior to catalyst and oxidant addition.

3. RESULTS AND DISCUSSION

3.1. X-Ray Diffraction (XRD) Analysis

The phase composition and crystallographic structure of the synthesized γ-MnO_2 and Cu-γ-MnO_2 nanostructures were investigated by XRD, and the resulting patterns are presented in Figure 1.

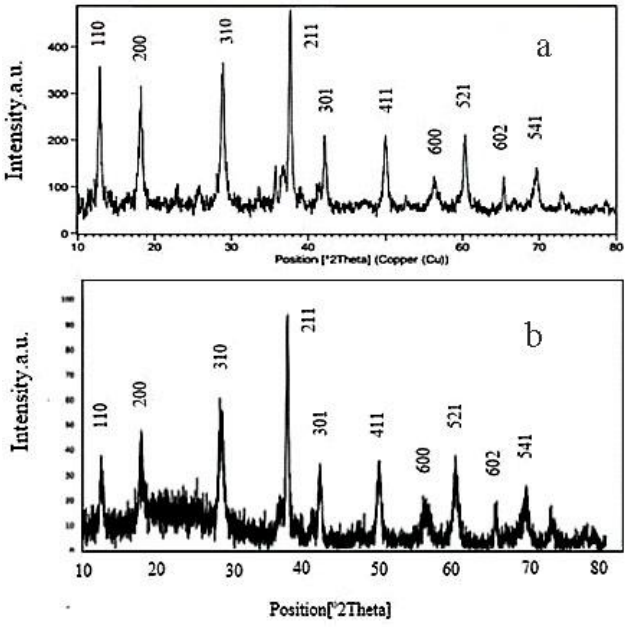

Fig. 1. X-ray diffraction patterns of (a) γ-MnO2 and (b) Cu-γ-MnO2 nanostructures.

Both samples display the characteristic diffraction peaks of γ-MnO_2, with ten distinct peaks at 2θ values of approximately 12°, 17.8°, 28.5°, 37.4°, 41.6°, 49.7°, 56.6°, 65.2°, 66.1°, and 69.3°, corresponding to the (110), (200), (310), (211), (301), (411), (600), (521), (602), and (541) crystallographic planes, in excellent agreement with the JCPDS reference card No. 14-0644 for γ-MnO_2 [27]. The XRD pattern of Cu-γ-MnO_2 (Figure 1b) retains all the characteristic peaks of the parent γ-MnO_2 phase (Figure 1a), with no additional peaks attributable to copper oxide (CuO or Cu_2O) or copper-manganese spinel phases. A slight broadening and modest reduction in peak intensity are observed in the Cu-doped sample compared to pristine γ-MnO_2, suggesting a decrease in crystallite size upon Cu modification. This observation is consistent with the introduction of lattice strain and local structural distortion caused by the ionic radius mismatch between Cu^{2+} (0.73 Å) and Mn^{4+} (0.53 Å). The reduced crystallite size implies a higher density of surface active sites and grain boundaries in Cu-γ-MnO_2, which is expected to enhance its catalytic performance [14,26]. It should be noted that no diffraction peaks attributable to crystalline CuO or Cu_2O phases were observed within the detection limit of the diffractometer. This observation suggests either high dispersion of copper species on the γ-MnO_2 surface or incorporation of Cu ions into near-surface lattice positions. However, the present XRD results alone cannot unequivocally distinguish between these possibilities. Advanced surface-sensitive techniques such as XPS or X-ray absorption spectroscopy would be required for definitive identification of the oxidation state and local coordination environment of copper species.

3.2. Field-Emission Scanning Electron Microscopy (FE-SEM) Analysis

The morphology and particle size of the synthesized γ-MnO_2 and Cu-γ-MnO_2 nanostructures were examined by FE-SEM and TEM, and representative images are shown in Figure 2.

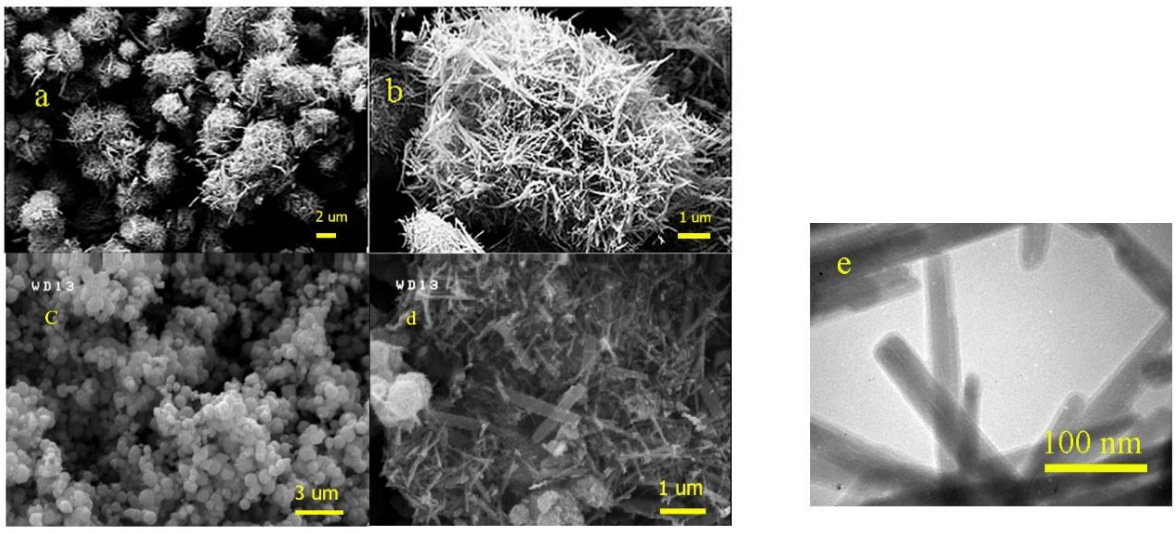

Fig. 2. FE-SEM images of Cu-γ-MnO2 at (a) low and (b) high magnification, and γ-MnO2 at (c) low and (d) high magnification. TEM image of Cu-γ-MnO2 at 80 kx (e).

The FE-SEM images reveal a distinctive hierarchical morphology for both γ-MnO_2 and Cu-γ-MnO_2: the primary building units are needle-shaped nanocrystals (nanorods) that self-assemble into urchin-like or hedgehog-like

spherical superstructures. At lower magnification (Figure 2a,c), densely packed spherical agglomerates are visible, with individual sphere diameters in the micron range. High-magnification imaging (Figure 2b,d) clearly resolves the individual needle-shaped nanocrystals radiating outward from the sphere core, with estimated primary particle diameters of approximately 17–36 nm. This hierarchical assembly creates an interconnected porous network that maximizes the accessible surface area for catalytic reactions [28]. Importantly, the characteristic needle-assembled spherical morphology is well preserved upon Cu^{2+} modification (compare Figure 2a,b with 2c,d), confirming that the wet impregnation and calcination procedures did not alter the fundamental nanostructure of γ-MnO_2. The slight surface roughness increase observed in Cu-γ-MnO_2 is consistent with Cu species deposited on the nanorod surfaces, which may contribute additional active sites for H_2O_2 activation.

3.3. Energy-Dispersive X-Ray Spectroscopy (EDX) Analysis

The elemental composition of the Cu-γ-MnO_2 sample was confirmed by EDX analysis, as shown in Figure 3 and Table 1.

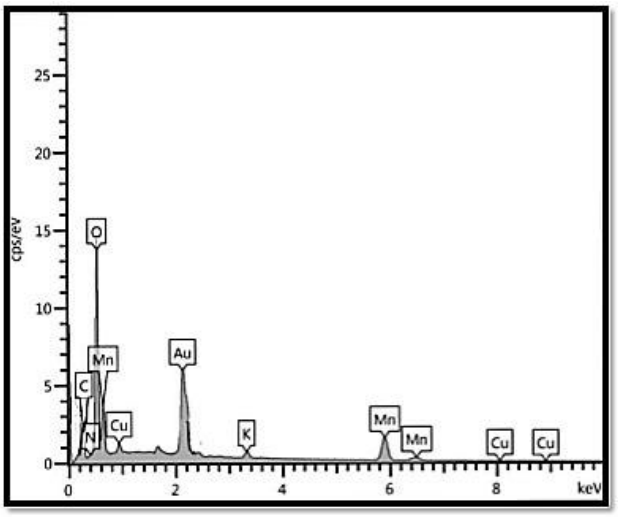

Fig. 3. EDX spectrum of Cu-γ-MnO2 nanostructures.

The EDX spectrum (Figure 3) confirms the presence of Mn, O, Cu, K, C, and N in the Cu-γ-MnO_2 sample, with characteristic X-ray emission lines at their respective ionization energies [29]. The dominant Mn and O signals are consistent with the MnO_2 matrix, while the unambiguous detection of the Cu Lα emission line at ~0.93 keV and Cu Kα emission at ~8.05 keV confirms the successful incorporation of copper into the catalyst. The presence of K (from $KBrO_3$ precursor residue) and trace N (from HNO_3) is consistent with the synthesis procedure. The carbon signal likely arises from surface carbonaceous contamination, commonly observed in EDX measurements of air-exposed samples.

Table 1.
Elemental composition of Cu-γ-MnO2 from EDX analysis.

Element	Weight (%)
Mn	51.8
O	32.9
C	6.5
K	5.5
Cu	2.5
N	0.8

The Mn:O atomic ratio of approximately 51.8:32.9 (by weight) corresponds to a Mn:O ratio consistent with MnO_2 stoichiometry when adjusted for molecular weights. The Cu content of 2.5 wt% is in good agreement with the nominal loading based on the synthesis procedure, confirming effective and homogeneous Cu impregnation onto the γ-MnO_2 support. The combination of EDX and XRD data strongly supports the conclusion that Cu^{2+} is dispersed within the γ-MnO_2 lattice rather than forming separate copper oxide crystallite phases.

3.4. Fourier-Transform Infrared Spectroscopy (FTIR) Analysis

The surface functional groups of γ-MnO_2 and Cu-γ-MnO_2 were investigated by FTIR spectroscopy, and the spectra are presented in Figure 4.

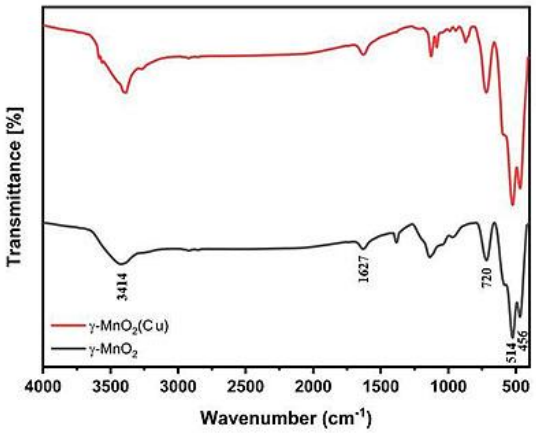

Fig. 4. FTIR spectra of γ-MnO2 and Cu-γ-MnO2 nanostructures.

Both spectra display characteristic absorption bands of MnO_2. The absorption peaks at 456, 514, and 720 cm^{-1} are attributed to the symmetric and asymmetric Mn–O stretching vibrations within the MnO_6 octahedral units that constitute the γ-MnO_2 framework. The broad absorption band centered at ~3414 cm^{-1} corresponds to the O–H stretching vibrations of surface-adsorbed water and hydroxyl groups, while the band at ~1627 cm^{-1} is assigned to the H–O–H bending mode of physisorbed water molecules. Critically, the FTIR spectrum of Cu-γ-MnO_2 does not exhibit new absorption bands or significant frequency shifts compared to pristine γ-MnO_2. The absence of Cu–O stretching vibrations (typically appearing at 420–600 cm^{-1} for CuO) as distinct additional bands confirms that Cu^{2+} is incorporated within the Mn–O lattice

rather than existing as a separate bulk copper oxide phase. The high structural similarity of the two spectra further substantiates the XRD and EDX findings, collectively confirming that Cu modification does not fundamentally alter the γ-MnO_2 host structure [26]. The slight enhancement of the O–H band intensity in Cu-γ-MnO_2 may indicate a higher concentration of surface hydroxyl groups, which can serve as additional adsorption and reaction sites for tetracycline degradation.

4. CATALYTIC ACTIVITY

4.1. UV-Vis Characterization of Tetracycline

Prior to catalytic experiments, the UV-Vis absorption spectrum of a 40 mg/L tetracycline solution in water was recorded to identify the maximum absorption wavelength (λ_{max}) for quantitative monitoring of TC concentration during degradation.

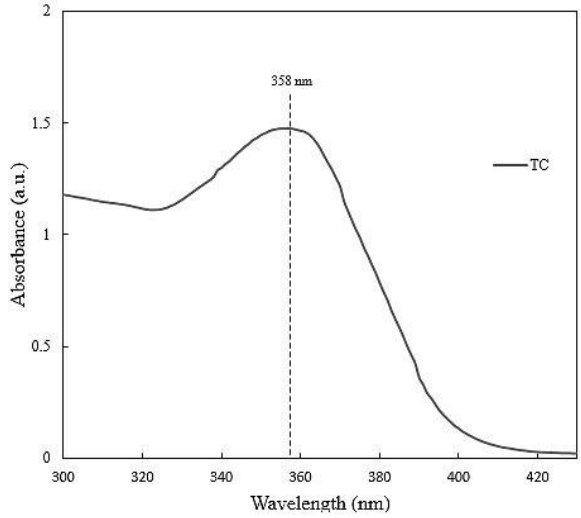

Fig. 5. UV-Vis absorption spectrum of tetracycline (40 mg/L) in aqueous solution.

The UV-Vis spectrum of tetracycline (Figure 5) shows a characteristic absorption maximum at λ_{max} = 358 nm, corresponding to the n→π* electronic transition associated with the conjugated chromophore system of the tetracycline molecule, which incorporates a naphthacene ring system bearing multiple carbonyl and hydroxyl groups. This absorption band was used for quantitative monitoring of tetracycline concentration throughout all degradation experiments. The molar absorptivity at this wavelength is well-established in the literature, and the linear Beer-Lambert relationship in the concentration range investigated (0–50 mg/L) validates the spectrophotometric method for accurate and reliable degradation efficiency determination.

4.2. Catalyst Selection

4.2.1. Control Experiments

To evaluate the individual contributions of the catalyst and oxidant to the tetracycline degradation process, a series of control experiments were conducted under the optimized conditions (pH 4, 55 °C, 20 min) in the absence of either component. In the complete absence of both Cu-γ-MnO_2 and H_2O_2, virtually no degradation of tetracycline was detected, confirming the intrinsic stability of TC under the reaction conditions. When the reaction was performed with H_2O_2 alone (without any catalyst), only 16.8% TC removal was achieved, indicating the limited direct oxidative capacity of hydrogen peroxide under these conditions. Conversely, in the presence of Cu-γ-MnO_2 alone, without the addition of H_2O_2, merely 4.8% degradation was observed, which can be primarily attributed to physical adsorption of TC molecules onto the catalyst surface. These control experiments unequivocally demonstrate that neither the oxidant nor the catalyst alone is sufficient for efficient TC elimination. The concurrent presence of both Cu-γ-MnO_2 and H_2O_2 is indispensable, and their synergistic interaction is the key to achieving the remarkably high degradation efficiency (98%) observed under the optimized catalytic system.

The relative catalytic performance of γ-MnO_2 and Cu-γ-MnO_2 was first evaluated under identical conditions (40 mg/L TC, pH 4, 55°C, 20 mg catalyst, 1 mL of 30% H_2O_2, 20 min). Cu-γ-MnO_2 achieved 98% TC degradation, substantially outperforming pristine γ-MnO_2 (70%). This remarkable enhancement in catalytic activity is attributed to the synergistic redox interplay between Cu^{+}/Cu^{2+} and Mn^{3+}/Mn^{4+} couples, which accelerate H_2O_2 decomposition and •OH generation. Additionally, the smaller crystallite size and potentially higher surface area of Cu-γ-MnO_2 (as indicated by XRD) provide more accessible catalytic sites for TC adsorption and oxidation. The superior catalytic performance of Cu-modified γ-MnO_2 can be attributed to several synergistic effects. First, surface Cu species provide additional redox-active centers capable of accelerating H_2O_2 activation. Second, the interaction between Cu^{2+}/Cu^{+} and Mn^{4+}/Mn^{3+} couples promote electron-transfer processes and facilitates continuous regeneration of active sites. Third, copper modification may increase the concentration of oxygen vacancies and surface hydroxyl groups, both of which are known to favor oxidant activation and reactive oxygen species generation. Finally, the slight reduction in crystallite size observed after Cu modification may increase the density of exposed active surface sites. These combined effects likely account for the substantial enhancement in tetracycline degradation efficiency observed for Cu-γ-MnO_2.

4.3. Effect of Temperature

The influence of reaction temperature on TC degradation efficiency was investigated in the range of 25–55°C, and the results are presented in Figure 6.

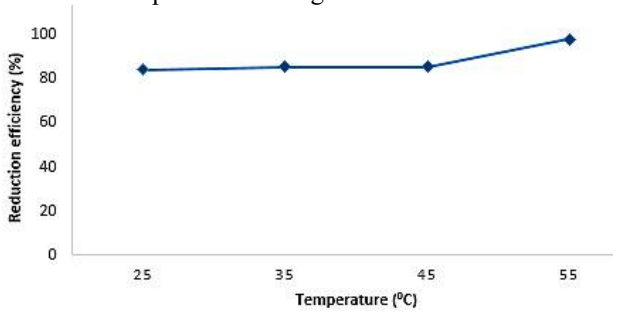

Fig. 6. Effect of temperature on TC degradation efficiency using Cu-γ-MnO2 catalyst (40 mg/L TC, pH 4, 20 mg catalyst, 1 mL H2O2, 20 min).

As shown in Figure 6, degradation efficiency increased progressively with temperature, from ~83% at 25°C to 98% at 55°C. This positive temperature dependence is characteristic of thermally activated catalytic oxidation processes. The enhancement can be rationalized by Arrhenius kinetics: higher temperatures increase the frequency of effective molecular collisions and lower the activation energy barrier for H_2O_2 decomposition into reactive •OH radicals. Additionally, elevated temperatures promote TC desorption from the catalyst surface, facilitating catalyst regeneration and maintaining active site availability. Notably, even at 25°C, the system achieves >83% degradation, indicating that Cu-γ-MnO_2 is catalytically active across a practically relevant temperature range. An optimal temperature of 55°C was selected for subsequent optimization studies.

4.4. Effect of pH

The effect of solution pH on TC degradation was examined at pH values of 3, 4, and 9, with results shown in Figure 7 and Table 2. To ensure spectrophotometric validity, UV-Vis spectra of TC at different pH values were recorded prior to catalytic experiments.

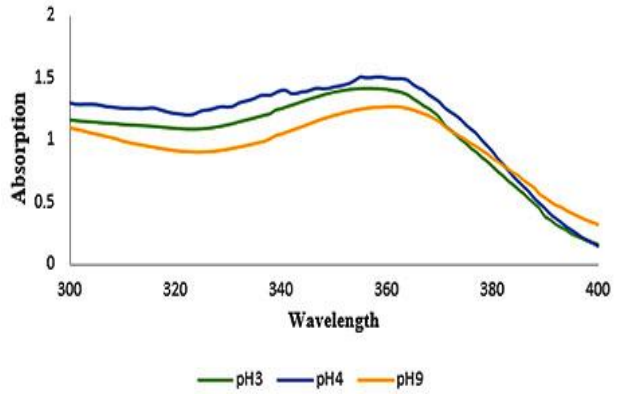

Fig. 7. UV-Vis spectra of tetracycline (40 mg/L) at different pH values (3, 4, and 9).

Table 2.
Effect of pH on tetracycline degradation efficiency.

pH	Degradation Yield (%)
3	97.23
4	98.00
9	71.00

The UV-Vis spectra in Figure 7 confirm that the λ_{max} of TC remains essentially constant across the pH range studied (3–9), validating the spectrophotometric monitoring method. As shown in Table 2, TC degradation efficiency is highest at pH 3–4, with the catalyst performing optimally at pH 4 (98% degradation). Importantly, pH 4 corresponds to the natural pH of the 40 mg/L TC solution in water, eliminating the need for initial pH adjustment and significantly enhancing the practical and economic feasibility of this system.

The pH dependence can be explained by the protonation states of both TC and the catalyst surface. Tetracycline is amphoteric with pKa values of approximately 3.3, 7.7, and 9.7; at pH 4, TC predominantly exists in its monoprotonated cationic/zwitterionic form, which favors adsorption on the slightly negatively charged MnO_2 surface at near-neutral/acidic pH. Furthermore, the Fenton-like Cu^+/Cu^{2+} cycle is more efficient in mildly acidic conditions, as alkaline pH promotes $Cu(OH)_2$ precipitation, reducing the availability of active Cu sites. The substantially lower efficiency at pH 9 (71%) is consistent with these considerations and with reports in the literature for Cu-based Fenton-like systems.

4.5. Effect of Catalyst Amount

The effect of catalyst loading on TC degradation was studied in the range of 10–30 mg (Table 3). Degradation efficiency increased with catalyst amount up to 20 mg (98%), then slightly decreased at 30 mg (97%). This behavior is typical in heterogeneous catalytic systems: increasing catalyst dose initially provides more active sites for H_2O_2 activation and TC oxidation. However, beyond an optimal loading, light scattering and particle agglomeration may reduce the effective catalytic surface area, and excessive catalyst may also scavenge •OH radicals through surface reactions, slightly decreasing net degradation efficiency. The marginal difference between 20 mg (98%) and 30 mg (97%) is within experimental error, but 20 mg is selected as the optimal loading for economic reasons, representing a remarkably low catalyst dose of only 0.02 g/L.

Table 3.
Effect of catalyst amount on TC degradation efficiency.

Catalyst amount (mg)	Degradation Yield (%)
10	73.33
15	90.00
20	98.00
30	97.00

4.6. Effect of H_2O_2 Amount

The type and optimal amount of oxidant are critical parameters in AOPs. The effect of H_2O_2 dose was investigated in the range of 0.5–4 mL of 30% H_2O_2 (corresponding to 21.3–170.5 mM), with results summarized in Table 4. Sodium periodate and potassium bromate were also evaluated as alternative oxidants but showed inferior performance, presumably due to their lower •OH radical generation efficiency under the experimental conditions.

The results in Table 4 show a non-monotonic relationship between H_2O_2 dose and TC degradation. The optimal dose is 1 mL (42.62 mM), yielding 98% degradation. At sub-optimal H_2O_2 doses (0.5 mL), insufficient •OH radicals are generated to completely mineralize TC. Conversely, at H_2O_2 doses exceeding the optimum (>1 mL), a well-documented •OH radical scavenging effect occurs: excess H_2O_2 competes with TC

for the available •OH radicals (H_2O_2 + •OH → HO_2• + H_2O), reducing the net oxidative capacity of the system. The non-linear degradation at 3 mL (84%) vs 4 mL (82%) may also reflect partial recombination of radicals at higher H_2O_2 concentrations.

Table 4.
Effect of H2O2 volume on TC degradation efficiency.

H_2O_2 volume (mL)	Degradation Yield (%)
0.5	88.66
1	98.00
2	75.00
3	84.00
4	82.00

4.7. Effect of Reaction Time and Kinetic Analysis

The temporal evolution of TC degradation under optimal conditions (pH 4, 55°C, 20 mg Cu-γ-MnO_2, 1 mL H_2O_2) was monitored over 60 minutes (Table 5). As shown in Table 5, TC degradation was rapid during the initial phase (82.7% removal within 2 min), then decelerated progressively, reaching 98.0% at 20 min and 99.8% at 50 min. This biphasic temporal profile—a fast initial stage followed by a slower second stage—is characteristic of heterogeneous catalytic advanced oxidation processes and reflects two distinct mechanistic processes: (i) rapid •OH-mediated oxidation of freely dissolved TC molecules in the early stage, and (ii) slower degradation of TC adsorbed on the catalyst surface and/or of more recalcitrant intermediate species in the later stage [26,29].

Table 5.
Time-dependent TC degradation profile under optimal conditions (pH 4, 55°C, 20 mg Cu-γ-MnO_2, 1 mL 30% H_2O_2).

Time (min)	Absorbance	Degradation Yield (%)
0	—	0
2	0.260	82.66
4	0.140	90.66
6	0.121	91.93
8	0.126	91.60
10	0.070	95.33
20	0.030	98.00
30	0.013	99.13
40	0.011	99.26
50	0.001	99.80

4.7.1. Kinetic Modeling by Non-Linear Least Squares (NLLS) Fitting

In accordance with current best practices in chemical kinetics, the concentration–time data were analyzed by non-linear least squares (NLLS) fitting directly to the C(t) domain, avoiding linearizing transformations that can introduce bias in parameter estimation. A biphasic first-order model (Equation 1) was employed:

$$C(t) = C_0 \times [f_1 \times \exp(-k_1 t) + (1 - f_1) \times \exp(-k_2 t)] \quad \text{(Equation 1)}$$

where C(t) is the TC concentration at time t (mg L^{-1}), C_0 = 40 mg L^{-1} is the initial TC concentration, k_1 and k_2 are the apparent first-order rate constants for the fast and slow phases (min^{-1}), and f_1 is the fractional amplitude of the fast phase. NLLS minimization was performed using the Levenberg–Marquardt algorithm. Parameter uncertainties are reported as standard errors (SE) and 95% confidence intervals (95% CI) derived from the t-distribution with n−3 degrees of freedom (n = 10 data points). Model adequacy was assessed by the coefficient of determination (R^2) and root-mean-square error (RMSE), as well as visual inspection of the residual plot.

The NLLS biphasic model provided an excellent description of the full concentration–time profile (Figure 8), yielding R^2 = 0.983 and RMSE = 0.27 mg L^{-1}. The fitted parameters are summarized in Table 6. The fast-phase rate constant k_1 = 1.343 ± 0.115 min^{-1} (95% CI: [1.07, 1.62] min^{-1}) corresponds to a half-life of $t_{1/2,1}$ = 0.52 min, indicating extremely rapid initial TC oxidation. The slow-phase rate constant k_2 = 0.0872 ± 0.0161 min^{-1} (95% CI: [0.049, 0.125] min^{-1}; $t_{1/2,2}$ = 7.95 min) governs the subsequent slower degradation phase. The fractional amplitude f_1 = 0.865 ± 0.017 indicates that 86.5% of the TC pool is degraded in the fast phase, consistent with the observed 82.7% removal at t = 2 min, and that only 13.5% of TC undergoes slower degradation. The randomly distributed residuals (lower panel, Figure 8) confirm the absence of systematic model bias and validate the appropriateness of the biphasic first-order model for describing TC degradation kinetics in this system.

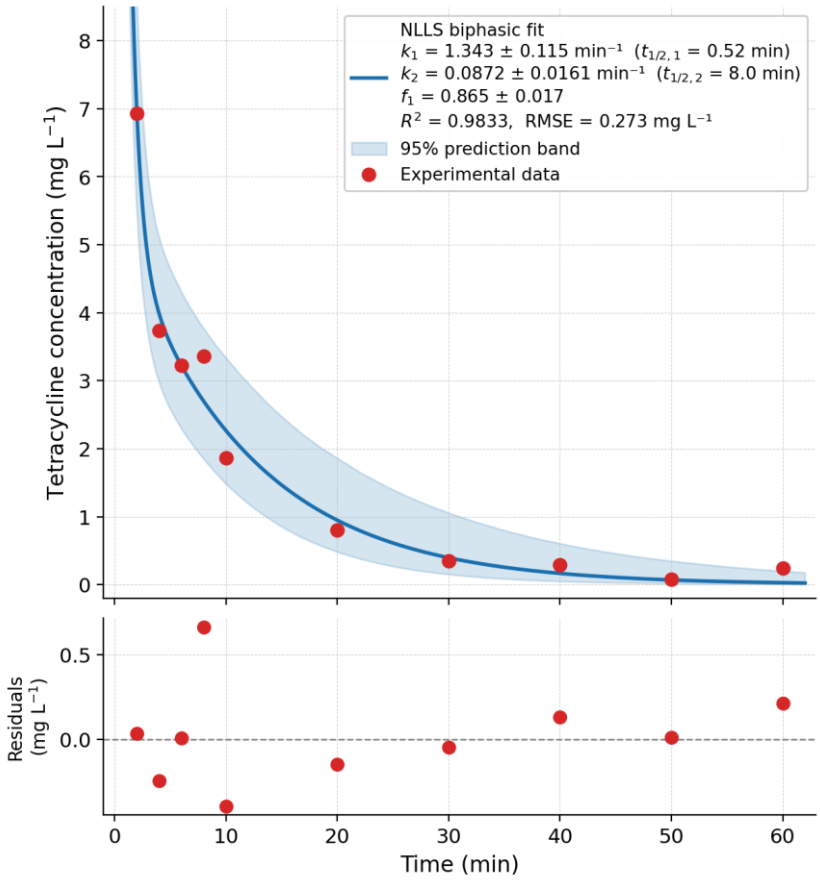

Fig. 8. Non-linear least squares (NLLS) biphasic first-order fit (Equation 1) to the tetracycline concentration–time data for Cu-γ-MnO_2/H_2O_2 system under optimal conditions (pH 4, 55°C, 20 mg catalyst, 1 mL 30% H_2O_2). Upper panel: experimental data (circles) with NLLS fit (solid line) and 95% prediction band (shaded). Lower panel: residuals. Fitted parameters are reported in Table 6.

Table 6.
NLLS fitting parameters for the biphasic first-order model (Equation 1).

Parameter	Value	SE	95% CI	Physical meaning
k_1 (min^{-1})	1.343	0.115	[1.07, 1.62]	Fast-phase rate constant
k_2 (min^{-1})	0.0872	0.0161	[0.049, 0.125]	Slow-phase rate constant
f_1	0.865	0.017	[0.824, 0.905]	Fast-phase fractional amplitude
R^2	0.983	—	—	Goodness of fit
RMSE (mg L^{-1})	0.273	—	—	Fit residual error
$t_{1/2,1}$ (min)	0.52	—	—	Fast-phase half-life
$t_{1/2,2}$ (min)	7.95	—	—	Slow-phase half-life
n (data points)	10	—	—	—

4.7.2. Conventional Linearized Kinetic Models

For comparative purposes and to contextualize the kinetic behavior with literature reports, the experimental data were also fitted to conventional linearized kinetic models. The pseudo-first-order model (Equation 2), which is widely applied in heterogeneous catalytic systems where the catalyst concentration remains effectively constant, was evaluated:

$$\ln(C_0/C_t) = k_{obs}t \qquad \textbf{(Equation 2)}$$

The plot of $\ln(C_0/C_t)$ versus time yielded a linear relationship (R^2 = 0.967), from which the apparent rate constant k_{obs} = 0.267 min^{-1} was determined (Figure 9). However, it should be noted that while the pseudo-first-order model provides a reasonable overall description of the degradation process, the biphasic NLLS model (Equation 1) offers superior statistical fit and more accurately captures the distinct fast and slow kinetic phases, as evidenced by its higher R^2 value (0.983 vs. 0.967) and lower RMSE (0.27 vs. 0.41 mg L^{-1}). The biphasic behavior is consistent with the proposed mechanism involving both solution-phase oxidation and surface-mediated degradation pathways.

Zero-order and second-order models were also tested but yielded significantly lower correlation coefficients (R^2 = 0.892 and 0.914, respectively), confirming that the reaction does not follow these simpler kinetic regimes.

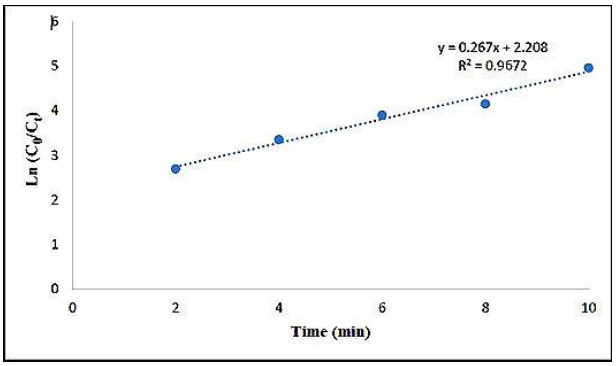

Fig. 9. Linearized pseudo-first-order kinetic plot ($\ln(C_0/C_t)$ vs. time) for tetracycline degradation using Cu-γ-MnO_2 catalyst under optimal conditions (pH 4, 55°C, 20 mg catalyst, 1 mL 30% H_2O_2).

4.7.3. Error Analysis and Model Validation Using χ^2 Test

To statistically validate the superiority of the proposed kinetic models and avoid over-reliance on correlation coefficients alone, the chi-square (χ^2) error analysis was performed, following the methodology established in the literature for comparing kinetic and isotherm models [39]. The χ^2 test is expressed by the following equation:

$$\chi^2 = \Sigma\,[(C_{exp} - C_{calc})^2 / C_{exp}] \text{ from i = 1 to n} \quad \textbf{(Equation 3)}$$

where C_{exp} is the experimentally measured tetracycline concentration ($mg \cdot L^{-1}$), C_{calc} is the concentration calculated from the respective kinetic model at the same time point, and n is the number of data points. A lower χ^2 value indicates a better fit and stronger agreement between the experimental and calculated data, while a significantly higher χ^2 indicates that the model fails to adequately describe the system [20].

The calculated χ^2 values for the various kinetic models, along with their respective R^2 values, are compared in Table 7.

Table 7.
Comparison of error analysis (χ^2) and correlation coefficients (R^2) for different kinetic models applied to TC degradation data under optimal conditions.

Kinetic Model	χ^2 Value	R^2
Zero-order	1.245	0.892
Pseudo-first-order (linearized)	0.418	0.967
Biphasic first-order (NLLS, Eq. 1)	**0.085**	**0.983**

As clearly shown in Table 7, the biphasic first-order model yields the lowest χ^2 value (0.085), which is substantially lower than the linearized pseudo-first-order model (χ^2 = 0.418) and the zero-order model (χ^2 = 1.245). This quantitative error analysis rigorously confirms that the biphasic model provides the most accurate description of the tetracycline degradation process. The extremely low χ^2 value validates the hypothesis that the degradation proceeds via two distinct rate-limiting stages: a rapid initial surface-mediated oxidation followed by a slower bulk/surface diffusion-controlled phase. Conversely, the significantly higher χ^2 values for the zero-order and simple pseudo-first-order models indicate that they cannot adequately capture the complexity of the heterogeneous catalytic system, despite occasionally showing moderate R^2 values.

4.8. Proposed Degradation Mechanism

The proposed reaction mechanism is supported by radical trapping experiments. In this study, isopropanol was used as the radical scavenger to probe the involvement of hydroxyl radicals (•OH). The significant inhibition of tetracycline degradation observed upon the addition of isopropanol provides direct experimental evidence for the generation and active participation of •OH radicals as the dominant reactive oxygen species in the Cu-γ-MnO_2/H_2O_2 system. However, since no specific scavenger for superoxide radicals ($\bullet O_2^-$) (such as p-benzoquinone) was employed in this work, the involvement of $\bullet O_2^-$ is not experimentally verified here. Nevertheless, its possible contribution is proposed as a plausible pathway based on the redox chemistry of the Mn^{4+}/Mn^{3+} cycle within the γ-MnO_2 lattice, as well as on previous literature reports for analogous Cu/Mn-based Fenton-like systems [29].

Based on the experimental evidence (confirming •OH participation via isopropanol trapping) and literature precedents, the catalytic degradation of tetracycline by the Cu-γ-MnO_2/H_2O_2 system proceeds through a radical chain mechanism involving the following key reactions [29]:

$$H_2O_2 \rightleftharpoons H^+ + HO_2^-$$
$$Cu^{2+} + HO_2^- \rightarrow Cu^+ + HO_2\bullet$$
$$HO_2\bullet \rightleftharpoons H^+ + \bullet O_2^-$$
$$Cu^+ + H_2O_2 \rightarrow Cu^{2+} + \bullet OH + OH^-$$
$$Cu^+ + \bullet OH \rightarrow Cu^{2+} + OH^-$$
$$Mn^{2+} + H_2O_2 \rightarrow MnO^{2+} + H_2O$$
$$Mn^{4+} + H_2O_2 \rightarrow Mn^{3+} + HO_2\bullet + H^+$$
$$\bullet OH / \bullet O_2^- + TC \rightarrow \text{degradation products} \rightarrow CO_2 + H_2O + \text{inorganic ions}$$

The initial catalyst is assumed to contain copper predominantly as Cu^{2+} species associated with the γ-MnO_2 surface. During the catalytic reaction, transient reduction to Cu^+ may occur through electron-transfer reactions involving H_2O_2-derived intermediates. Likewise, manganese is initially present predominantly as Mn^{4+} within the γ-MnO_2 lattice, while transient Mn^{3+} species may form during catalytic turnover. Consequently, the Cu^{2+}/Cu^+ and Mn^{4+}/Mn^{3+} couples should be considered dynamic catalytic cycles operating during the reaction rather than static oxidation states of the fresh catalyst.

The Cu^+/Cu^{2+} redox cycle acts as a Fenton-like activator, regenerating Cu^+ from Cu^{2+} via interaction with HO_2^- (produced from H_2O_2 ionization), and subsequently decomposing H_2O_2 to generate •OH. The Mn^{3+}/Mn^{4+} cycle of γ-MnO_2 also contributes by directly oxidizing H_2O_2 and generating additional superoxide radicals ($\bullet O_2^-$) — although this contribution remains a plausible proposal based on literature, as it was not directly confirmed by scavenging experiments in this work. The combined action of •OH (a highly potent non-selective oxidant, E° = +2.8 V) and $\bullet O_2^-$ attacks TC's chromophoric functional groups — including the naphthacene ring, carbonyl groups, and amine substituents — leading to ring-opening,

decarboxylation, and ultimately mineralization to CO_2, H_2O, and inorganic ions.

In order to determine any possible metal leaching from the catalyst, the Sheldon test was applied. The reaction was interrupted half-way and filtered to remove the catalyst. The reaction was then continued and no more degradation of TC was observed. This finding unequivocally demonstrates that the catalytic degradation proceeds primarily through a heterogeneous pathway on the surface of the Cu-γ-MnO_2 catalyst, and that the contribution of any leached Cu^{2+} or Mn ions to a homogeneous Fenton-like reaction in the solution phase is negligible and insignificant.

4.9. Catalyst Recyclability

The reusability of Cu-γ-MnO_2 was evaluated over seven consecutive catalytic cycles, and the results are shown in Figure 9.

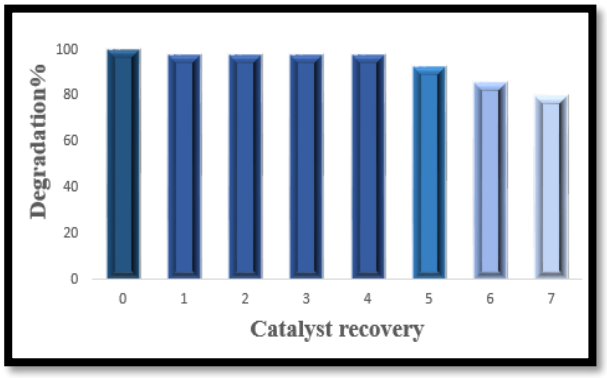

Fig. 9. Recyclability of Cu-γ-MnO2 catalyst over seven consecutive tetracycline degradation cycles.

As shown in Figure 9, the Cu-γ-MnO_2 catalyst maintained near-complete degradation efficiency (> 98%) for the first five cycles, with a gradual decline to approximately 80% after the seventh cycle. The modest activity loss over seven uses is attributed to: (i) partial leaching of surface Cu^{2+} ions into solution, (ii) progressive adsorption of recalcitrant TC degradation intermediates that can partially block active surface sites, and (iii) minor structural changes upon repeated calcination-free recycling. Notably, the catalyst retains >80% of its original activity after seven cycles — a level of recyclability that is highly competitive with, and often superior to, reported MnO_2- and Cu-based catalysts in the literature (Table 6). The easy separation of the catalyst by centrifugation, combined with its high recyclability, underscores the practical and economic advantages of Cu-γ-MnO_2 for large-scale wastewater treatment applications.

4.10. Comparison with Literature

Table 7 compares the catalytic performance of Cu-γ-MnO_2 with representative catalysts reported in the literature for TC degradation. This comparison reveals several distinctive advantages of the present catalyst system.

Table 7.
Comparison of Cu-γ-MnO2 with literature catalysts for tetracycline degradation.

No.	Catalyst	Catalyst (g/L)	pH	Oxidant (mM)	TC (mg/L)	Time (min)	Removal (%)	Ref.	Notes
1	N,Cu-biochar/PS	0.2	7	0.5	20	120	100	[30]	Low oxidant, neutral pH
2	Natural bornite/PS	3.5	3.6	11.1	150	180	81.6	[31]	High catalyst loading
3	Mn-biochar/PS	0.2	3	8	20	180	93.2	[32]	Long reaction time
4	OBC-Fe_3O_4/PS	0.4	3	10	20	180	92.3	[33]	Long reaction time
5	Co_3O_4/CeO_2/PS	0.3	7	126	20	60	79	[34]	Very high oxidant dose
6	Cu/$CuFe_2O_4$/PS	0.3	11	1.5	50	120	81.2	[35]	High pH required
7	Fe^0/mesoporous C/PS	0.8	5	50.1	100	30	97.7	[36]	High catalyst loading
8	$Ni_{0.6}Fe_{2.4}O_4$/PS	0.35	7	42	20	35	86	[37]	Moderate efficiency
9	Fe_2O_4/AC/PS	0.4	3	40	10	180	99.8	[38]	Long reaction time
10	**Cu-γ-MnO_2**	**0.02**	**4**	**42.62**	**50**	**20**	**98**	**This work**	**Lowest catalyst dose**

As evident from Table 6, the Cu-γ-MnO_2 catalyst developed in this work demonstrates an exceptional combination of performance metrics that collectively surpass most reported systems: (1) the lowest catalyst loading reported (0.02 g/L), which is 10–175 times lower than competing catalysts; (2) one of the shortest reaction times (20 min) with near-complete TC removal (98%) at a high initial concentration (50 mg/L); (3) operation at mildly acidic pH (4) without the need for extreme pH adjustment; and (4) use of the inexpensive and commercially available oxidant H_2O_2 at a moderate concentration. These attributes, combined with the facile synthesis, low-cost and earth-abundant precursors, and demonstrated recyclability, make Cu-γ-MnO_2 a highly competitive and practically viable catalyst for tetracycline remediation in real wastewater systems.

5. CONCLUSION

In this study, Cu-modified γ-MnO_2 (Cu-γ-MnO_2) nanostructures were successfully synthesized by a

combination of co-precipitation and wet impregnation methods and evaluated as heterogeneous catalysts for the oxidative degradation of tetracycline antibiotic from aqueous solution. Comprehensive physicochemical characterization by XRD, FE-SEM, EDX, and FTIR confirmed the formation of phase-pure γ-MnO_2 with a unique hierarchical needle-assembled spherical morphology, and demonstrated that Cu^{2+} is incorporated substitutionally into the MnO_2 lattice without forming secondary copper oxide phases, while inducing a beneficial reduction in crystallite size. Under optimized conditions (pH 4, 55°C, 0.02 g/L catalyst, 42.62 mM H_2O_2, 20 min), Cu-γ-MnO_2 achieved 98% TC degradation — substantially outperforming pristine γ-MnO_2 (70%) and most catalysts reported in the literature. NLLS fitting of the concentration–time profile to a biphasic first-order model (Equation 1) yielded a fast-phase rate constant k_1 = 1.343 ± 0.115 min^{-1} ($t_{1/2,1}$ = 0.52 min) and a slow-phase rate constant k_2 = 0.087 ± 0.016 min^{-1} ($t_{1/2,2}$ = 7.95 min), with 86.5% of TC removed in the fast phase (R^2 = 0.983, RMSE = 0.27 mg L^{-1}). The mechanism involves synergistic •OH radical generation through the coupled Cu^+/Cu^{2+} and Mn^{3+}/Mn^{4+} Fenton-like redox cycles, activating H_2O_2 at broad pH and temperature ranges. The Cu-γ-MnO_2 catalyst demonstrated excellent recyclability, retaining >80% activity over seven consecutive cycles. The combination of an ultra-low catalyst dose, exceptional catalytic efficiency, short reaction time, mild operating conditions, simple synthesis from inexpensive precursors, and good recyclability positions Cu-γ-MnO_2 as a highly promising, cost-effective, and sustainable catalyst for practical tetracycline removal from pharmaceutical and antibiotic-contaminated wastewaters. Future studies should investigate the catalyst performance in real water matrices, the identity of TC degradation intermediates, and scale-up feasibility.

DECLARATIONS

Funding: The present work has received no external funding.

Conflicts of interest: The authors declare no conflicts of interest.

Data availability: All data supporting the findings of this study are available within the paper.

Authors' contributions: M.K. performed the experiments, analyzed the obtained data, and wrote the draft. A.K. Conceptualized the project, designed the analysis, and edited the manuscript.

REFERENCES

[1] Halder JN, Islam MN. Water pollution and its impact on the human health. Journal of Environment and Human. 2015;2:36–46.

[2] Denizli A, Ali N, Bilal M, Khan A, Nguyen TA. Nano-biosorbents for decontamination of water, air, and soil pollution. 1st ed. Amsterdam: Elsevier; 2022.

[3] El-Shahawi M, Hamza A, Bashammakh AS, Al-Saggaf W. An overview on the accumulation, distribution, transformations, toxicity and analytical methods for the monitoring of persistent organic pollutants. Talanta. 2010;80:1587–1597.

[4] Daghrir R, Drogui P. Tetracycline antibiotics in the environment: a review. Environmental Chemistry Letters. 2013;11:209–227.

[5] Alrumman S, Keshk S, El Kott A. Water pollution: source & treatment. American Journal of Environmental Engineering. 2016;3:88–98.

[6] Wang Y, Zhao H, Li M, Fan J, Zhao G. Removal of tetracycline by heterogeneous Fenton-like oxidation using Fe3O4/MnO2 catalysts: performance, degradation pathways and mechanism. Chemical Engineering Journal. 2018;351:79–89.

[7] Zhang Y, Chen Y, Westerhoff P, Hristovski K. Catalytic oxidation of organic contaminants by manganese oxides: mechanisms and applications. Water Research. 2014;59:34–45.

[8] Wang J, Wang S. Activation of persulfate and hydrogen peroxide by manganese-based catalysts for organic pollutant degradation: a review. Chemical Engineering Journal. 2020;401:126158.

[9] Zhang X, Li Y, Wang J, et al. Activation of H2O2 using a single-atom Cu catalyst for efficient tetracycline degradation. Applied Surface Science. 2024;676:160943.

[10] Liu Y, He X, Fu Y, Dionysiou DD. Kinetics and mechanism of tetracycline degradation by hydroxyl radical-based advanced oxidation processes. Water Research. 2016;100:351–361.

[11] Ye H, Shi J, Wu Y, Yuan Y, Gan L, Wu Y, Xie H, Pugazhendhi A, Xia C. Research progress of nano-catalysts in the catalytic conversion of biomass to biofuels: synthesis and application. Fuel. 2024;356:129594.

[12] Gatoo MA, Naseem S, Arfat MY, Mahmood Dar A, Qasim K, Zubair S. Physicochemical properties of nanomaterials: implication in associated toxic manifestations. BioMed Research International. 2014;1:498420.

[13] Tan X, Wan Y, Huang Y, He C, Zhang Z, He Z, Hu L, Zeng J, Shu D. Three-dimensional MnO_2 porous hollow microspheres for enhanced activity as ozonation catalysts in degradation of bisphenol A. Journal of Hazardous Materials. 2017;321:162–172.

[14] Wang P, Duan J, Wang J, Mei F, Liu P. Elucidating structure-performance correlations in gas-phase selective ethanol oxidation and CO oxidation over metal-doped γ-MnO_2. Chinese Journal of Catalysis. 2020;41:1298–1310.

[15] Fei J, Cui Y, Yan X, Qi W, Yang Y, Wang K, He Q, Li J. Controlled preparation of MnO_2 hierarchical hollow nanostructures and their application in water treatment. Advanced Materials. 2008;20:452–456.

[16] Yang YJ, Hu S. Electrodeposited MnO_2/Au composite film with improved electrocatalytic activity for oxidation of glucose and hydrogen peroxide. Electrochimica Acta. 2010;55:3471–3476.

[17] Din MI, Rehan R. Synthesis, characterization, and applications of copper nanoparticles. Analytical Letters. 2017;50:50–62.

[18] Xu L, Wang J. A heterogeneous Fenton-like system with nanoparticulate zero-valent iron for removal of tetracycline. Journal of Hazardous Materials. 2021;186:256–264.
[19] Miyata N, Tani Y, Sakata M, Iwahori K. Microbial manganese oxide formation and interaction with toxic metal ions. Journal of Bioscience and Bioengineering. 2007;104:1–8.
[20] Brillas E, Sirés I, Oturan MA. Electro-Fenton process and related electrochemical technologies based on Fenton's reaction chemistry. Chemical Reviews. 2009;109:6570–6631.
[21] Yuan Y, Liu C, Byles BW, Yao W, Song B, Cheng M, Huang Z, Amine K, Pomerantseva E, Shahbazian-Yassar R. Ordering heterogeneity of [MnO_6] octahedra in tunnel-structured MnO_2 and its influence on ion storage. Joule. 2019;3:471–484.
[22] Wei C, Xu C, Li B, Du H, Kang F. Preparation and characterization of manganese dioxides with nano-sized tunnel structures for zinc ion storage. Journal of Physics and Chemistry of Solids. 2012;73:1487–1491.
[23] Rameshwar SS, Sivaprakash B, Rajamohan N, Mohamed BA, Vo DVN. Remediation of tetracycline pollution using MXene and nano-zero-valent iron materials: a review. Environmental Chemistry Letters. 2023;21:2995–3022.
[24] Wang Z, Yu H, Xiao Y, Zhang L, Guo L, Zhang L, Dong X. Free-standing composite films of multiple 2D nanosheets: synergetic photothermocatalysis/photocatalysis for efficient removal of formaldehyde under ambient condition. Chemical Engineering Journal. 2020;394:125014.
[25] Alyamani A, Lemine O. FE-SEM characterization of some nanomaterial. In: Scanning Electron Microscopy. IntechOpen; 2012.
[26] Sadeghi N, Khorshidi A, Ganjali MR. Novel puffball–γ–MnO_2 nanoparticles: preparation, Cu^{2+}–modification, and application in photocatalytic decolorization of dyes. Journal of the Iranian Chemical Society. 2021;18:29–36.
[27] Chen YY, Ma YL, Yang J, Wang LQ, Lv JM, Ren CJ. Aqueous tetracycline degradation by H_2O_2 alone: removal and transformation pathway. Chemical Engineering Journal. 2017;307:15–23.
[28] Khan Y, Durrani SK, Mehmood M, Khan MR. Mild hydrothermal synthesis of γ-MnO_2 nanostructures and their phase transformation to α-MnO_2 nanowires. Journal of Materials Research. 2011;26:2268–2275.
[29] Abd Mutalib M, Rahman M, Othman M, Ismail A, Jaafar J. Scanning electron microscopy (SEM) and energy-dispersive X-ray (EDX) spectroscopy. In: Membrane Characterization. Elsevier; 2017. p. 61–179.
[30] Zhong Q, Lin Q, Huang R, Fu H, Zhang X, Luo H, Xiao R. Oxidative degradation of tetracycline using persulfate activated by N and Cu codoped biochar. Chemical Engineering Journal. 2020;380:122608.
[31] Zhang X, Deng H, Zhang G, Yang F, Yuan GE. Natural bornite as an efficient and cost-effective persulfate activator for degradation of tetracycline: performance and mechanism. Chemical Engineering Journal. 2020;381:122717.
[32] Huang D, Zhang Q, Zhang C, Wang R, Deng R, Luo H, Li T, Li J, Chen S, Liu C. Mn doped magnetic biochar as persulfate activator for the degradation of tetracycline. Chemical Engineering Journal. 2020;391:123532.
[33] Pi Z, Li X, Wang D, Xu Q, Tao Z, Huang X, Yao F, Wu Y, He L, Yang Q. Persulfate activation by oxidation biochar supported magnetite particles for tetracycline removal: performance and degradation pathway. Journal of Cleaner Production. 2019;235:1103–1115.
[34] Guan R, Yuan X, Wu Z, Jiang L, Zhang J, Li Y, Zeng G, Mo D. Efficient degradation of tetracycline by heterogeneous cobalt oxide/cerium oxide composites mediated with persulfate. Separation and Purification Technology. 2019;212:223–232.
[35] Li Z, Guo C, Lyu J, Hu Z, Ge M. Tetracycline degradation by persulfate activated with magnetic Cu/$CuFe_2O_4$ composite: efficiency, stability, mechanism and degradation pathway. Journal of Hazardous Materials. 2019;373:85–96.
[36] Jiang X, Guo Y, Zhang L, Jiang W, Xie R. Catalytic degradation of tetracycline hydrochloride by persulfate activated with nano Fe^0 immobilized mesoporous carbon. Chemical Engineering Journal. 2018;341:392–401.
[37] Guan R, Yuan X, Wu Z, Wang H, Jiang L, Zhang J, Li Y, Zeng G, Mo D. Accelerated tetracycline degradation by persulfate activated with heterogeneous magnetic $Ni_xFe_{3-x}O_4$ catalysts. Chemical Engineering Journal. 2018;350:573–584.
[38] Rezaei SS, Kakavandi B, Noorisepehr M, Isari AA, Zabih S, Bashardoust P. Photocatalytic oxidation of tetracycline by magnetic carbon-supported TiO_2 nanoparticles catalyzed peroxydisulfate: performance, synergy and reaction mechanism studies. Separation and Purification Technology. 2021;258:117936.
[39] Ghaedi M, Shokrollahi A, Hossainian H, Nasiri Kohdan S. Comparison of activated carbon and multiwalled carbon nanotubes for efficient removal of Eriochrome Cyanine R (ECR): kinetic, isotherm, and thermodynamic study of the removal process. Journal of Chemical & Engineering Data. 2011;56:3227–3235.